SLAC-PUB-1057
(TH) and (EXP)
June 1972

ANALYSIS OF γp REACTIONS IN THE LPS FRAMEWORK AT $E_\gamma = 6 - 18$ GeV*

F. F. Liu**, M. Davier, I. Derado***, D. C. Fries†, R. F. Mozley, A. C. Odian, J. Park***, W. P. Swanson, F. Villa and D. Yount††

Stanford Linear Accelerator Center
Stanford University, Stanford, California 94305

Abstract

The reactions $\gamma p \to \pi^+\pi^- p$ and $\gamma p \to \pi^+\pi^-\pi^+\pi^- p$ in the energy range $E_\gamma = 6 - 18$ GeV from the SLAC 2-meter streamer chamber are analyzed in terms of the longitudinal-phase-space (LPS) method. The 3-body LPS hexagonal plot shows accumulations which reflect the dominant diffractive ρ^0 production. The five-body final state is divided into sixteen LPS sectors. The partial cross sections, invariant-mass and momentum-transfer distributions of the four populous sectors are presented and discussed. Within this framework, we attempt to isolate and study the dissociations $(\gamma \to \pi^+\pi^-)$, $(\gamma \to \pi^+\pi^-\pi^+\pi^-)$ and the double dissociations $(\gamma \to \pi^+\pi^-,\ p \to p\pi^+\pi^-)$. The proton dissociation $(p \to p\pi^+\pi^-)$ is found to be in approximate agreement with results from πp and pp reactions. Assuming that Pomeron exchange dominates, this result is consistent with Pomeron factorization.

(Submitted to Nuclear Physics B)

---

* Work supported by the U. S. Atomic Energy Commission.
** Physics Department, California State College, San Bernardino, California 92407, U.S.A.
*** Max Planck Institut für Physik und Astrophysik, Munich, Germany.
† Institut für Experimentale Kernphysik, Universität Karlsruhe, Germany.
†† Department of Physics and Astronomy, University of Hawaii, Honolulu, Hawaii 96822, U.S.A.

1. Introduction

In an N-body final state, (3N - 4) variables are required to describe an event, so that simple invariant-mass and four-momentum-transfer distributions are not efficient in providing a brief, yet comprehensive profile of a reaction with more than three particles. These distributions are large in number, and their interpretation is complicated by the multiple combinations of final-state particles. Motivated by the fact that the transverse momenta of final-state particles in high-energy reactions are small, Van Hove has formulated a method of analysis[1,2] using the cm longitudinal momenta of the particles as variables, thus reducing the dimensionality of the phase space. The longitudinal momentum also serves as a tag to identify each of the final-state particles according to its ordering within an event. The reduced phase space can be further divided into sectors according to the signs of the longitudinal momenta. Events in a sector may then be interpreted intuitively by means of a simple dominant graph[3,4].

This method has been successfully applied to 3, 4, and 5-body final states in pion-induced reactions[3,5,6,7]. In this paper, we apply the longitudinal-phase-space (LPS) method to the photo-induced reactions yielding 3 and 5 particles:

$$\gamma p \rightarrow \pi^+ \pi^- p, \tag{1}$$

$$\gamma p \rightarrow \pi^+ \pi^- \pi^+ \pi^- p. \tag{2}$$

The data are from the SLAC 2-meter streamer chamber, exposed to a bremsstrahlung beam of 18 GeV maximum energy. The 5-prong events come from the entire sample of film (600,000 triads), and the 3-prong events are from about half of the same sample. The numbers of events in the range $E_\gamma = 6 - 18$ GeV are 1795 and 1140 for reactions (1) and (2), respectively. The data are corrected for varying geometrical and triggering efficiencies by

assigning an individual weight to each event. These and other experimental details†[8,9] and related analyses[10,11,12] based on these data are described elsewhere.

2. Three-Body Final State: $\gamma p \rightarrow \pi^+ \pi^- p$

In the LPS analysis for three outgoing particles, each event is plotted as a point whose perpendicular distances to three inclined axes define the cm longitudinal momenta of the particles[1,2], as shown in fig. 1. Because of energy and momentum conservation, the distribution of points is bounded by a regular hexagon of side $(s/3)^{\frac{1}{2}}$, where s is the total cm energy squared. In this experiment, this incident beam has a bremsstrahlung energy spectrum, so that the side of the hexagon is different for each event. To accommodate the events in a large energy range, we normalize each event by dividing the longitudinal momenta of the final-state particles by $(s/3)^{\frac{1}{2}}$, so that all hexagons have unit side. Each point in the plot can be described in polar coordinates ω and r as shown in fig. 1a. The projection on ω preserves the correlation between the longitudinal momenta of the particles, and the projection on r reveals the peripherality of the interaction.

Most of the events in fig. 1 are concentrated near the boundary of the plot and in the sextant where both π^+ and π^- are in the forward direction and the proton backwards. The projections are given in figs. 2 and 3. With increasing E_γ the distribution in r moves closer to the boundary, and there is progressive depopulation outside the ω range corresponding to forward π^+ and π^-. This reaction has been analyzed in a conventional way[10,13,14,15,16,17] and found to be dominated by the diffraction dissociation ($\gamma \rightarrow \pi^+ \pi^-$). This main process of reaction (1) thus manifests itself clearly in a marked accumulation of events in one sextant of the hexagonal plot.

† The experimental arrangement is similar to that described in ref. 8).

3. Five-Body Final State: $\gamma p \rightarrow \pi^+\pi^-\pi^+\pi^- p$

The longitudinal phase space for five particles is represented on a closed 3-dimensional polyhedron in a 4-dimensional space[1,2]. Here it is more conventional to use the reduced longitudinal momenta defined in the cm system $X_i = q_i/(\frac{1}{2}\Sigma_{j=1}^{5}|q_j|)$, where q_i is the longitudinal momentum of particle i. These reduced momenta satisfy the constraints

$$\sum_{i=1}^{5}|X_i| = 2, \qquad \sum_{i=1}^{5} X_i = 0$$

independent of incident beam energy. The pions of the same charge are then ordered according to their reduced longitudinal momenta such that $X_f^{\pm} > X_s^{\pm}$. Here the superscript refers to the meson charge, and the subscript "f" refers to the particle having greater X than particle "s" of the same charge. X_p denotes the reduced longitudinal momentum of the proton.

The reduced longitudinal-momentum distributions are shown in fig. 4. It is observed that the protons are sharply peaked in the backward direction near $X_p \simeq -1.0$. As expected, the "f" pions are overwhelmingly in the forward region $X > 0.0$, although they are not pushed as sharply to the kinematical limit as in the case of the protons. There is no qualitative difference between the X_f^+ and X_f^-. The "s" pions are accumulated near X=0.0. Both X_s^+ and X_s^- have a tail extending towards negative X, but the X_s^+ distributions are noticeably broader than those of X_s^-.

Figure 5 shows the corresponding transverse-momentum P_T distributions. All five are qualitatively similar, although the average P_T for π_s^+ is somewhat lower than for other pions, presumably due to its connection with the Δ^{++}. The average transverse momentum for all pions is $\langle P_T \rangle = 0.353 \pm 0.004$ GeV/c, and for protons is $\langle P_T \rangle = 0.413 \pm 0.009$ GeV/c. These averages are similar to those found in other high-energy reactions.

The $\pi^+\pi^-$ invariant-mass distributions are shown in fig. 6, where we distinguish between "f" and "s" pions. There is a prominent ρ^o signal in three of the four $\pi^+\pi^-$ pairings, and it is especially strong in the $\pi_f^+\pi_f^-$ combination, suggesting the concept of a "leading ρ^o" related to the incident photon. The relative lack of ρ^o signal found in $\pi_s^+\pi_f^-$ (as compared to $\pi_f^+\pi_s^-$) can be ascribed to the strong Δ^{++} which would usually involve the slower π_s^+. This picture is confirmed in fig. 7, which shows the $p\pi_f^+$ and $p\pi_s^+$ mass distributions. The Δ^{++} signal is very prominent in the $p\pi_s^+$ combinations but rather weak in $p\pi_f^+$.

We have made a detailed search for accumulations in different sectors of longitudinal phase space. In so doing, sixteen sectors of LPS are defined by grouping the five particles into all possible combinations of forward and backward-going particles. As shown in Table 1, four of these sectors contain 81% of the events. All four populous sectors are characterized by the selection $X_p < 0$ and $X_f^+, X_f^- > 0$. This result suggests the picture of the photon interacting with the proton target and then materializing into two fast-going pions as the proton continues in its original direction. An analysis of reaction (2) is thus made manageable because of the accumulation of events in these restricted LPS sectors. The four sectors with significant numbers of events are differentiated according to whether X_s^+ and X_s^- are positive or negative:

$X_f^+, X_f^-, X_s^+, X_s^- > 0;$	$X_p < 0$	Sector I
$X_f^+, X_f^-, X_s^+ > 0;$	$X_s^-, X_p < 0$	Sector II
$X_f^+, X_f^- > 0;$	$X_s^+, X_s^-, X_p < 0$	Sector III
$X_f^+, X_f^-, X_s^- > 0;$	$X_s^+, X_p < 0$	Sector IV

Diagrams associated with each of the four sectors are shown in fig. 8 and are denoted as $\gamma p \rightarrow (\pi_f^+ \pi_f^- \pi_s^+ \pi_s^-)(p)$, $\gamma p \rightarrow (\pi_f^+ \pi_f^- \pi_s^+)(\pi_s^- p)$, $\gamma p \rightarrow (\pi_f^+ \pi_f^-)(\pi_s^+ \pi_s^- p)$, and $\gamma p \rightarrow (\pi_f^+ \pi_f^- \pi_s^-)(\pi_s^+ p)$, respectively. As used in connection with fig. 8, one may regard these diagrams as only a mnemonic for an unambiguous classification scheme. However, to the extent that these diagrams also represent real physical processes, we would expect that these sectors would be rich in events arising from the corresponding process. The thrust of this paper is to show that this is plausible by further study of each sector. Pomeron exchange is allowed in the diagrams for sectors I and III, but forbidden for sectors II and IV because charge is exchanged. Additional processes may be present in these four sectors, but the steep t-dependences, the low-mass enhancements and the resonances found suggest that these quasi-two-body diagrams must in fact play a significant role. The invariant-mass distributions in the four sectors as suggested by these diagrams are given in fig. 9 for $E_\gamma = 6 - 18$ GeV. Previous analysis[11] of reaction (2) has shown a strong ρ^o signal in $\pi^+\pi^-$ combinations (see fig. 6), a strong Δ^{++} signal in $p\pi^+$ combinations (see fig. 7) and a broad enhancement in $\pi^+\pi^-\pi^+\pi^-$ mass at about 1600 MeV. These resonances are clearly seen in the sectors III, IV, and I, respectively, in fig. 9. A natural consequence of this division into sectors is the suppression of backgrounds, allowing signals such as the ρ^o and Δ^{++} to be more readily associated with the corresponding diagrams. This has been demonstrated above for the simpler case of reaction (1).

The four-momentum-transfer $t' \equiv |t - t_{min}|$ distributions between γ and the forward-going particle groups are given in fig. 10 for $E_\gamma = 6 - 18$ GeV. The slope parameters obtained by fitting over the range $t' = 0.0 - 0.48$ $(GeV/c)^2$ are 5.6 ± 0.6, 4.0 ± 1.2, 5.6 ± 0.8, and 6.3 ± 0.7 $(GeV/c)^{-2}$ for the four sectors,

respectively. Over the fitted range, the slope parameters for sectors I and III are consistent with diffraction dissociation, as in reaction (1). In sectors II and IV pion exchange is expected to dominate, and the difference in slopes is probably connected with the differing $N\pi$ mass distributions; the $p\pi_s^+$ mass spectrum is strongly dominated by Δ^{++}, whereas the $p\pi^-$ shows a much broader distribution.

The partial cross sections for these sectors are given in fig. 11 as functions of photon energy. We see that the partial cross sections for $\gamma p \to (\pi_f^+\pi_f^-)(\pi_s^+\pi_s^-p)$ in sector III, $\gamma p \to (\pi_f^+\pi_f^-\pi_s^-)(\pi_s^+p)$ in sector IV, $\gamma p \to (\pi_f^+\pi_f^-\pi_s^+\pi_s^-)(p)$ in sector I are about equal and significantly larger than that of $\gamma p \to (\pi_f^+\pi_f^-\pi_s^+)(\pi_s^-p)$ in sector II.

4. Sector I: Photon Dissociation

At energies above 6 GeV, reaction (1) is dominated (to about 85%) by the ρp final state. Analyses of reaction (1) have demonstrated[10,13,14,15,16,17] the importance of a diagram (fig. 12b) in which a Pomeron is exchanged. Therefore we look in sector I for the analogous dissociation of photon into four pions (fig. 12a).

A low-mass enhancement (about 1600 MeV) of $M(\pi^+\pi^-\pi^+\pi^-)$ is clearly seen in sector I of (fig. 9a). The t'-distribution between γ and $\pi^+\pi^-\pi^+\pi^-$ in this sector is given in fig. 10. The slope parameter of 5.6 ± 0.6 $(GeV/c)^{-2}$ is consistent with the Pomeron-exchange diagram (fig. 12b). It is then reasonable to consider events in this sector to be mainly from the dissociation $\gamma \to \pi^+\pi^-\pi^+\pi^-$. Reference (11) provides further evidence for diffraction dissociation of the photon into four pions in reaction (2) in a different type of analysis. There is now new evidence from a Frascati electron-positron colliding beam experiment for a broad four-pion peak at about the same mass 1600 MeV[18,19,20].

Referring to fig. 12, we study the dissociation of γ into pions by taking the ratio of the partial cross sections of reaction (2) in sector I to that of the corresponding sextant in fig. 1 ($\omega = 120^{o} - 180^{o}$). These two LPS regions are "corresponding" in the sense that the proton is backward and all pions are forward in both. We define $R_1 = \sigma[\gamma p \rightarrow (\pi^+\pi^-\pi^+\pi^-)(p)]/\sigma[\gamma p \rightarrow (\pi^+\pi^-)(p)]$. Within the LPS framework, we do not attempt to subtract backgrounds in computing R_1, but include all the events in the indicated phase-space regions. The ratios R_1 are 0.064 ± 0.010, 0.087 ± 0.014, and 0.079 ± 0.013 at the mean photon energies of 8, 12, and 16 GeV, respectively. Within errors, these ratios are consistent with no energy variation.

5. Sector III: Double Dissociation and Pomeron Factorization

Since we know that the γ dissociates into $\pi^+\pi^-$ strongly through Pomeron exchange in reaction (1) and that the proton dissociates[21,22] into a complex of isobars including the N*(1470), and N*(1700), in πp, pp, and Kp interactions, sector III is a natural place to look for double dissociation. The mass plots of $\pi_f^+\pi_f^-$ and $\pi_s^+\pi_s^-p$ in sector III are given in fig. 9d,e. We see a strong ρ^o peak in the $\pi_f^+\pi_f^-$ effective-mass distribution, and a broad low-mass enhancement at about 1400 - 2200 MeV in $M(\pi_s^+\pi_s^-p)$, qualitatively similar to that seen in other experiments, although distinct peaks are not apparent with the statistics available. An analysis of the decay angular distribution of the $\pi_f^+\pi_f^-$ shows a strong $\sin^2\theta_H$ component in the helicity frame (fig. 13), similar to that found in reaction (1)[10,13,14,15,16,17]. The invariant-momentum-transfer t' distribution for this sector is shown in fig. 10. For no selection on the effective masses $M(\pi_s^+\pi_s^-p)$ or $M(\pi_f^+\pi_f^-)$, the slope parameter is $B = 5.6 \pm 0.8$ $(GeV/c)^{-2}$. This agrees with that found in the reaction $\pi^-p \rightarrow \pi^-(\pi^+\pi^-p)$: $B = 5.3 \pm 0.3$, 5.6 ± 0.3 $(GeV/c)^{-2}$ at incident pion momenta 11 and 16 GeV/c, respectively[3,4].

Guided by the picture of a γ materializing into a $\pi_f^+\pi_f^-$ pair and thus treating the pion pair as equivalent to the beam particle, we study the dissociation $(p \to \pi^+\pi^- p)$ in this sector, as motivated by fig. 14a. We do this by forming the ratio $R_2 = \sigma [\gamma p \to (\pi_f^+\pi_f^-)(\pi_s^+\pi_s^- p)] / \sigma [\gamma p \to (\pi^+\pi^-)(p)]$. The ratios R_2, obtained with only the longitudinal-momenta selection as described and no background correction, are given in Table 2. When we further require these pion pairs to be in the ρ^o band (660 - 840 MeV) and apply corrections for an estimated background in both reactions, we obtain smaller ratios R_2' also given in Table 2.

We now compare this ratio R_2 to that of other hadron-induced reactions (see fig 14b), in particular to $R_3^{\pm} = \sigma[\pi^{\pm} p \to (\pi^{\pm})(\pi^+\pi^- p)] / \sigma[\pi^{\pm} p \to \pi^{\pm} p]$ and $R_4 = \sigma[pp \to (p)(\pi^+\pi^- p)] / \sigma[pp \to pp]$ at various energies.† These ratios are calculated with the same forward-backward selection on the particles as we have used here and are given in Table 2 for comparison. The agreement between these ratios from four different types of reactions is reasonably good, considering that only simple selections are made. This qualitative agreement is consistent with the hypothesis of Pomeron factorization[23, 24].

† These results are communicated to us by Prof. L. Van Hove. Dr. W. Kittel of CERN computed the values for $R_2^{\pm}$ at 16 GeV/c from the data of the Aachen-Berlin-Bonn-CERN-Cracow-Heidelberg-Warsaw Collaboration. See refs. 3 and 5. Prof. S. Ratti of Milano computed the values of $R_2^{\pm}$ at 11 GeV/c from the same collaboration. Dr. N. K. Yamdagni of CERN computed the values for R_3 at 10, 19 and 24.8 GeV/c from the data of Cambridge-Hamburg, the Scandinavian Collaboration and Rutgers-Columbia, respectively.

Predictions for diagram III (fig. 8) have been calculated by Wolf[25], based on the assumption of Pomeron factorization. He predicts a slope parameter of about 5.4 $(GeV/c)^{-2}$ and a cross section of 1 - 1.5 μb in this energy range. His slope parameter agrees with the observed 5.6 ± 0.8 $(GeV/c)^{-2}$. Figure 11 shows a cross section for the corresponding LPS sector of about 1 μb, but a direct quantitative comparison of cross sections is not meaningful because Wolf's calculation includes all decay modes†† of the N*'s produced at the lower vertex of diagram III, and does not make use of the LPS selection used in this paper.

6. Summary

We have analyzed γp reactions in different regions of longitudinal phase space for both 3 and 5-body final states. In the 3-body final state we find an accumulation of events in the LPS sextant corresponding to the well-known diffractive rho photoproduction. For the 5-body final state, the average transverse momentum of protons and pions is small (about 0.35 - 0.40 GeV/c), comparable to that found in πp and pp reactions, thus justifying the use of the LPS method. Only four of the 16 LPS sectors defined are populated with significant numbers of events, making this analysis tractable. Examination of these four sectors shows that the important resonances of this reaction appear prominently in different sectors. We exploit this division into sectors to obtain information on photon dissociation into four pions, by comparing the 3 and 5-body reactions in corresponding LPS regions. Evidence for double dissociation ($\gamma \rightarrow \pi^+\pi^-$, $p \rightarrow \pi^+\pi^- p$) is found in

†† Assuming that the $I = \frac{1}{2}$ isobars decay equally into $N\pi$ and $N\pi\pi$, and that the $\pi\pi$ system in the $N\pi\pi$ decay has I = 0 (or 1), Wolf's cross section should be divided by a factor of 3 (or 6) to compare with data of reaction (2).

one of the LPS sectors. A comparison of ($p \rightarrow \pi^+\pi^- p$) in this sector is made with similar results from πp and pp reactions. The agreement obtained is consistent with the idea of Pomeron factorization.

Acknowledgements

We wish to thank the Streamer-Chamber technical staff and our scanning, measuring, and data-analysis staff for their essential contributions to this work. It is a pleasure to thank the accelerator and computer operating groups and the machine shops for their assistance. We are deeply indebted to Professor L. Van Hove for his informative correspondence regarding this analysis and his communication of results on πp and pp data. We wish to thank Professor S. Ratti and Dr. W. Kittel for their kind permission to quote results on πp data.

References

1. L. Van Hove, Phys. Letters 28B (1969) 429.
2. L. Van Hove, Nucl. Phys. B9 (1969) 331.
3. W. Kittel, S. Ratti, and L. Van Hove, Nucl. Phys. B30 (1971) 333.
4. L. Van Hove, Phys. Reports 1C (1971) 347.
5. J. V. Beaupre, et al., CERN/D. Ph. II/PHYS 72-1.
6. J. Ballam, G. B. Chadwick, Z. G. T. Guiragossián, W. B. Johnson, D.W. G.S. Leith, and K. Moriyasu, Phys. Rev. D4 (1971) 1946.
7. G. Tomasini, E. Bassler, M. Sahini, P. Schilling, P. Borzatta, G. Cecchet, L. Liotta, S. Ratti, A. Daudin, M. L. Faccini, and M. A. Jabiol, Nuovo Cimento 7A (1972) 651.
8. M. Davier, I. Derado, D. Drickey, D. Fries, R. Mozley, A. Odian, F. Villa, and D. Yount, Phys. Rev. D1 (1970) 790.
9. D. C. Fries, M. Davier, I. Derado, F. F. Liu, R. F. Mozley, A. Odian, J. Park, W. P. Swanson, F. Villa, and D. Yount, in preparation.
10. J. Park, M. Davier, I. Derado, D. C. Fries, F. F. Liu, R. F. Mozley, A. Odian, W. P. Swanson, F. Villa, and D. Yount, Nucl. Phys. B36 (1972) 404.
11. M. Davier, I. Derado, D. C. Fries, F. F. Liu, R. F. Mozley, A. Odian, J. Park, W. P. Swanson, F. Villa, and D. Yount. Contribution to the 1971 International Symposium on Photon and Electron Interactions at High Energies, Cornell, August, 1971.
12. W. P. Swanson, M. Davier, I. Derado, D. C. Fries, F. F. Liu, R. F. Mozley, A. C. Odian, J. Park, F. Villa, and D. E. Yount, Phys. Rev. Letters 27 (1971) 1472.

13. Cambridge Bubble Chamber Group, Phys. Rev. 146 (1966) 994.

14. Aachen-Berlin-Bonn-Hamburg-Heidelberg-München Collaboration, Phys. Rev. 175 (1968) 1669.

15. H. H. Bingham, W. B. Fretter, K. C. Moffeit, W. J. Podolsky, M. S. Rabin, A. H. Rosenfeld, R. Windmolders, J. Ballam, G. B. Chadwick, R. Gearhart, Z. G. T. Guiragossián, M. Menke, J. J. Murray, P. Seyboth, A. Shapira, C. K. Sinclair, I. O. Skillicorn, and G. Wolf, Phys. Rev. Letters 24 (1970) 955.

16. Y. Eisenberg, B. Haber, E. E. Ronat, A. Shapira, Y. Stahl, G. Yekutieli, J. Ballam, G. B. Chadwick, M. M. Menke, P. Seyboth, S. Dagan, and A. Levy, Phys. Rev. D5 (1972) 15.

17. J. Ballam, G. B. Chadwick, R. Gearhart, Z. G. T. Guiragossián, J. J. Murray, P. Seyboth, C. K. Sinclair, I. O. Skillicorn, H. Spitzer, G. Wolf, H. H. Bingham, W. B. Fretter, K. C. Moffeit, W. J. Podolsky, M. S. Rabin, A. H. Rosenfeld, R. Windmolders, and R. H. Milburn, Phys. Rev. D5 (1972) 545.

18. G. Barbarino, M. Grilli, E. Iarocci, P. Spillantini, V. Valente, R. Visentin, F. Ceradini, M. Conversi, L. Paoluzi, R. Santonico, M. Nigro, L. Trasatti, and G. T. Zorn, Lett. Nuovo Cimento 3 (1972) 689.

19. A. Bramon and M. Greco, Lett. Nuovo Cimento 1 (1971) 739.

20. A. Bramon and M. Greco, Lett. Nuovo Cimento 3 (1972) 693.

21. J. G. Rushbrooke, Proceedings of the Fourteenth International Conference on High Energy Physics, Vienna, Austria, September 1968, p. 158.

22. D.R.O. Morrison, Rapporteur talk, in Proceedings of the Fifteenth International Conference on High Energy Physics, Kiev, USSR, 1970 (Moscow, 1971).

23. P.G.O. Freund, Phys. Rev. Letters 21 (1968) 1375.

24. L. Van Hove, Ann. Phys. (N.Y.) 66 (1971) 449.

25. G. Wolf, Nuclear Physics B26 (1971) 317.

Table 1

Partition of the Reaction $\gamma p \to \pi^+\pi^-\pi^+\pi^-$ into LPS Sectors. $E_\gamma = 6 - 18$ GeV.

Proton backward				Proton forward			
LPS sector		Raw	Weighted[a]	LPS sector		Raw	Weighted[a]
(forward)	(backward)	events	events	(forward)	(backward)	events	events
$(\pi_f^+\pi_f^-\pi_s^+\pi_s^-)$	(p)	264	321 ± 20	(p)	$(\pi_f^+\pi_f^-\pi_s^+\pi_s^-)$	3	5.2 ± 3.0
$(\pi_f^+\pi_f^-\pi_s^+$)	(π_s^-p)	146	192 ± 16	(π_f^-p)	($\pi_f^+\pi_s^-\pi_s^+$)	13	19.3 ± 5.5
$(\pi_f^+\pi_f^-\pi_s^-$)	(π_s^+p)	274	356 ± 22	(π_f^+p)	($\pi_s^+\pi_f^-\pi_s^-$)	15	25.5 ± 6.7
$(\pi_f^+\pi_f^-$)	($\pi_s^+\pi_s^-$p)	266	384 ± 24	($\pi_f^+\pi_f^-$p)	($\pi_s^+\pi_s^-$)	27	42.2 ± 8.4
$(\pi_f^+\pi_s^+$)	($\pi_f^-\pi_s^-$p)	17	26 ± 7	($\pi_f^-\pi_s^-$p)	($\pi_f^+\pi_s^+$)	6	9.6 ± 4.2
$(\pi_f^-\pi_s^-$)	($\pi_f^+\pi_s^+$p)	52	75 ± 11	($\pi_f^+\pi_s^+$p)	($\pi_f^-\pi_s^-$)	3	4.4 ± 2.6
(π_f^+)	($\pi_s^+\pi_f^-\pi_s^-$p)	16	27 ± 7	($\pi_f^+\pi_f^-\pi_s^-$p)	(π_s^+)	4	6.1 ± 3.2
(π_f^-)	($\pi_s^-\pi_f^+\pi_s^+$p)	30	49 ± 9	($\pi_f^+\pi_f^-\pi_s^+$p)	(π_s^-)	4	5.2 ± 2.7

a) Weighted to correct for chamber geometry and trigger efficiency.

Table 2

Comparison of the ratios of partial cross sections in γp, πp and pp reactions.

Sector ratio \ Energy	E_γ = 6 - 10 GeV	E_γ = 10 - 14 GeV	E_γ = 14 - 18 GeV
$R_2 = \frac{\sigma[\gamma p \to (\pi_f^+\pi_f^-)(\pi_s^+\pi_s^- p)]}{\sigma[\gamma p \to (\pi^+\pi^-)(p)]}$	0.096 ± 0.014	0.079 ± 0.013	0.079 ± 0.015
$R_2' = \frac{\sigma[\gamma p \to (\pi_f^+\pi_f^-)_\rho(\pi_s^+\pi_s^- p)]}{\sigma[\gamma p \to (\pi^+\pi^-)_\rho (p)]}$	0.053 ± 0.014	0.035 ± 0.014	0.055 ± 0.024
Pion momentum:	11 GeV/c		16 GeV/c
$R_3^+ = \frac{\sigma[\pi^+ p \to \pi^+(\pi^+\pi^- p)]}{\sigma[\pi^+ p \to \pi^+ p]}$	0.061 ± 0.006		0.063 ± 0.003
$R_3^- = \frac{\sigma[\pi^- p \to \pi^-(\pi^+\pi^- p)]}{\sigma[\pi^- p \to \pi^- p]}$	0.052 ± 0.005		0.059 ± 0.003
Proton momentum:	10 GeV/c	19 GeV/c	24.8 GeV/c
$R_4 = \frac{\sigma[pp \to p(\pi^+\pi^- p)]}{\sigma[pp \to pp]}$	0.064 ± 0.007	0.061 ± 0.008	0.060 ± 0.009

Figure Captions

1. Van Hove hexagonal plot for $\gamma p \rightarrow \pi^+\pi^- p$ for three E_γ intervals. In fig. 1a, the coordinate system for ω and r is shown together with the reduced hexagon of unit side. All three show the envelope calculated for the upper value of the corresponding E_γ interval and for actual particle masses.
2. Reduced r distributions for the reaction $\gamma p \rightarrow \pi^+\pi^- p$.
3. Distributions in ω for the reaction $\gamma p \rightarrow \pi^+\pi^- p$.
4. Reduced-longitudinal-momentum (X) distributions for $\gamma p \rightarrow \pi_f^+\pi_f^-\pi_s^+\pi_s^- p$.
5. Transverse-momentum (P_T) distributions for $\gamma p \rightarrow \pi_f^+\pi_f^-\pi_s^+\pi_s^- p$.
6. Invariant-mass $M(\pi^+\pi^-)$ distributions for $\gamma p \rightarrow \pi_f^+\pi_f^-\pi_s^+\pi_s^- p$.
7. Invariant-mass $M(p\pi^+)$ distributions for $\gamma p \rightarrow \pi_f^+\pi_f^-\pi_s^+\pi_s^- p$.
8. Sectors I-IV defined as bounded quadrants in the X_s^+, X_s^- plane. The diagrams likely to be important in each sector are shown. $\mathbb{P}$ and M denote Pomeron and meson, respectively.
9. Invariant-mass distributions for $\gamma p \rightarrow \pi_f^+\pi_f^-\pi_s^+\pi_s^- p$ within the four sectors.
10. Four-momentum-transfer $t' = t - t_{min}$ distributions between the photon and the forward-going particle groups in the four sectors for $E_\gamma = 6 - 18$ GeV. The line is fitted for t' in the range $0.0 - 0.48$ $(GeV/c)^2$.
11. Partial cross sections for each of the four sectors as a function of E_γ.
12. Diagrams motivating the search for photon dissociation into four pions.
13. Helicity angular distribution of π_f^- in the $(\pi_f^+\pi_f^-)$ rest frame. (a) Sector III, all events; (b) as (a), but with additional mass selection $M(\pi_f^+\pi_f^-)$ between 600 and 900 MeV. The curves are $\sin^2\theta_H$, normalized to the numbers of events.
14. Diagrams motivating the comparison in proton dissociation between (a) γp reactions, and (b) Ap reactions, where A stands for any incident particle.

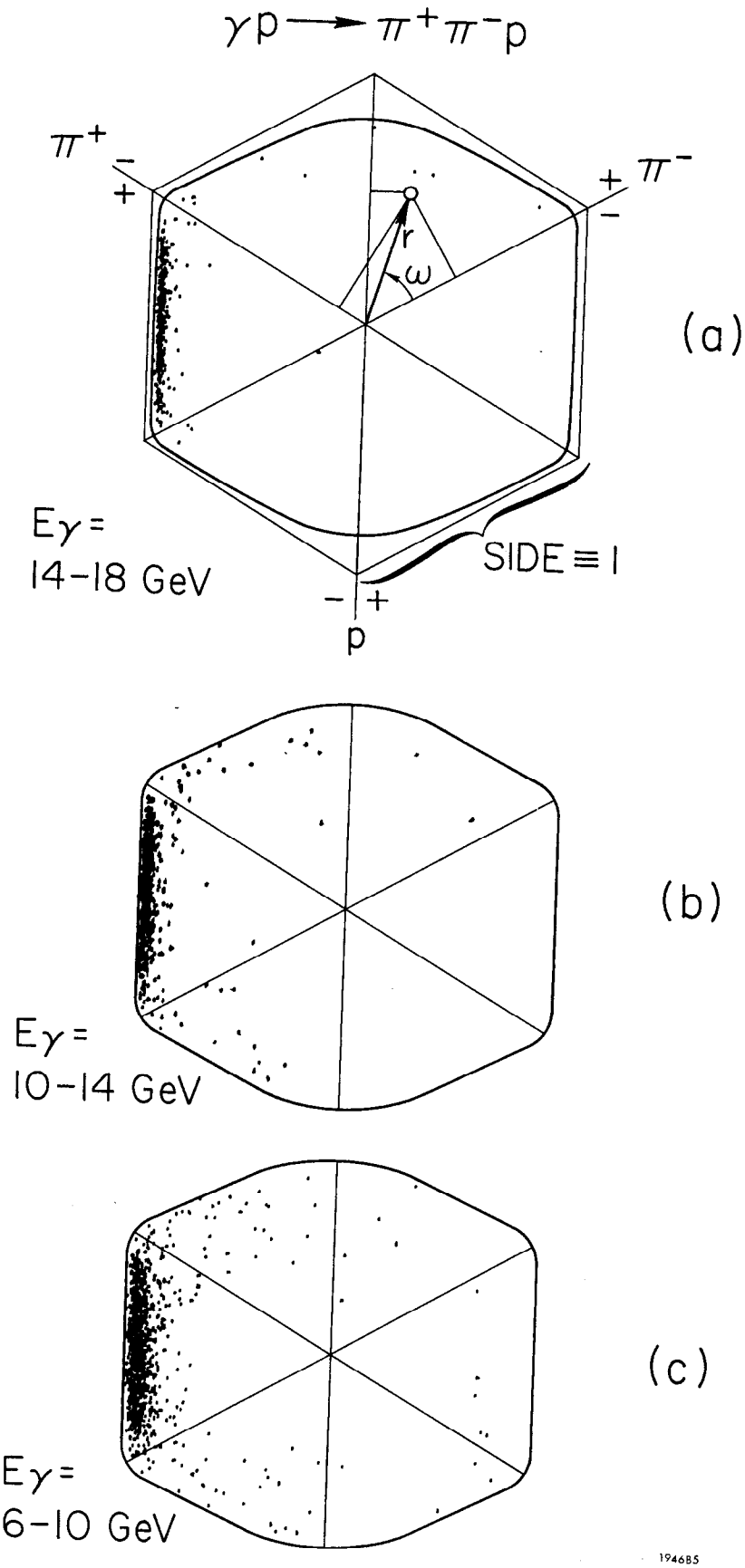
γp → π⁺π⁻p
π⁺
π⁻
r
ω
(a)
Eγ =
14–18 GeV
SIDE ≡ 1
p
(b)
Eγ =
10–14 GeV
(c)
Eγ =
6–10 GeV
194685

Fig. 1

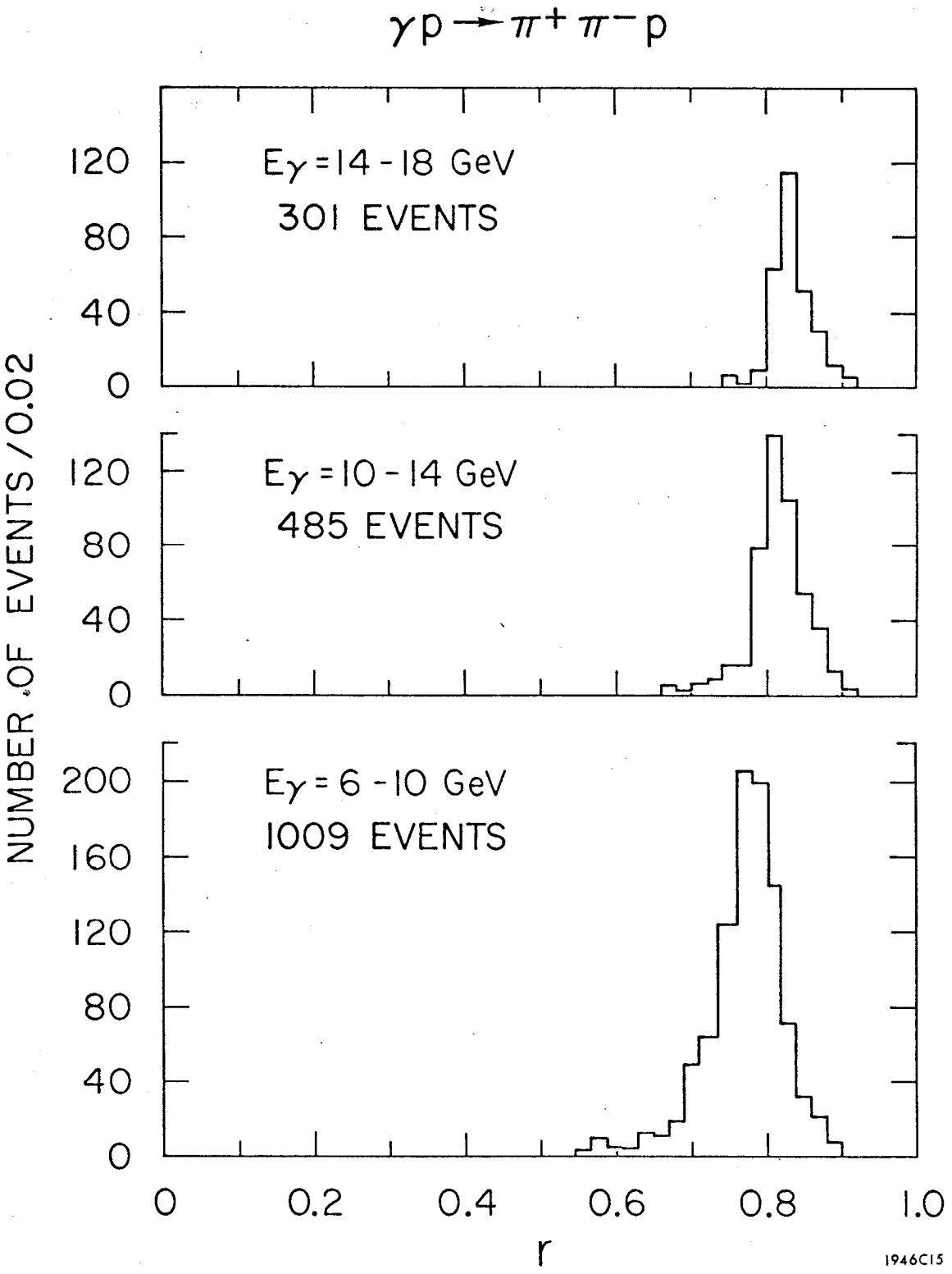
γp → π+ π− p
Eγ = 14 - 18 GeV
301 EVENTS
Eγ = 10 - 14 GeV
485 EVENTS
Eγ = 6 - 10 GeV
1009 EVENTS
NUMBER OF EVENTS / 0.02
120
80
40
0
120
80
40
0
200
160
120
80
40
0
0
0.2
0.4
0.6
0.8
1.0
r
1946C15

Fig. 2

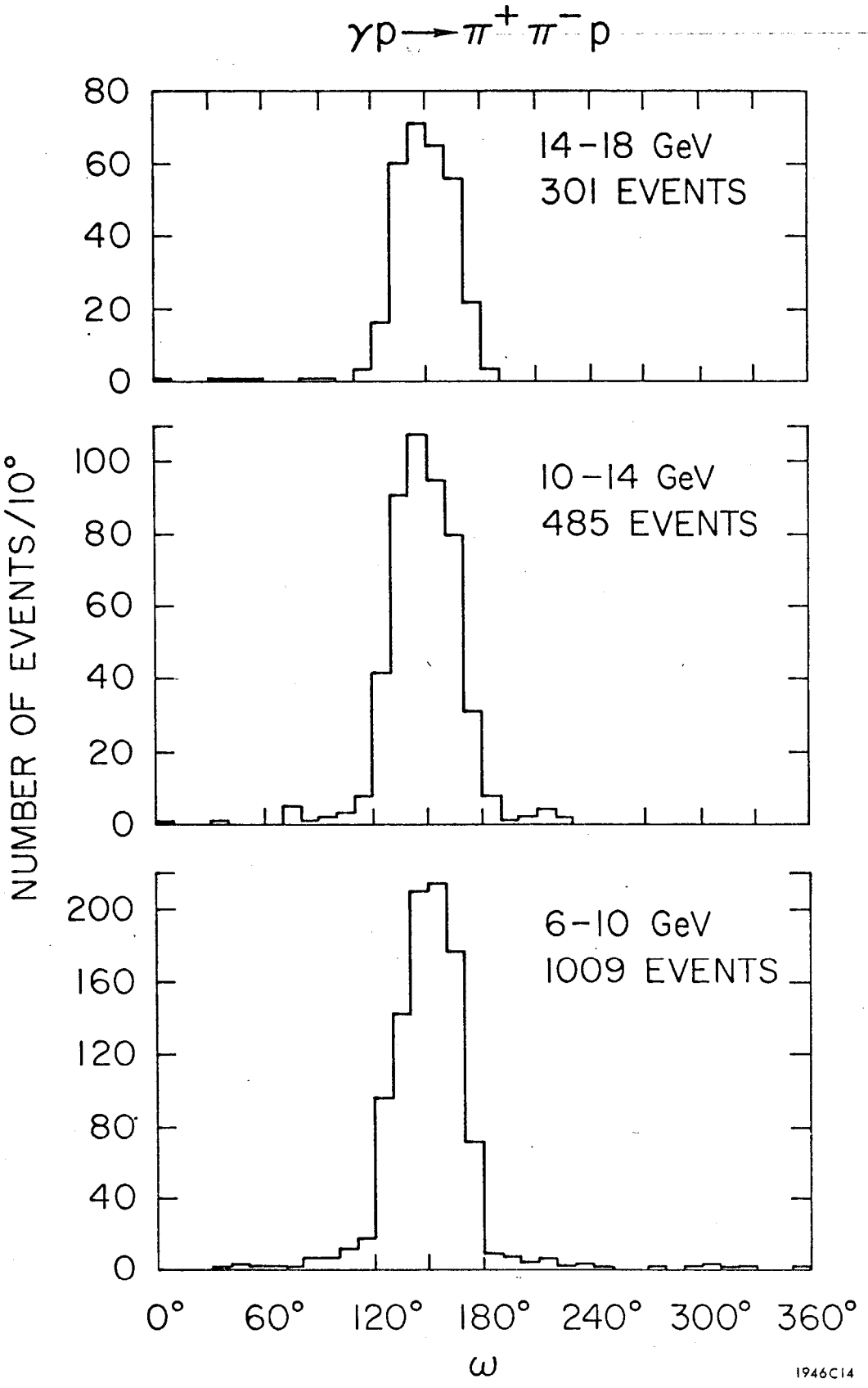
$\gamma p \rightarrow \pi^+ \pi^- p$
14-18 GeV
301 EVENTS
10-14 GeV
485 EVENTS
6-10 GeV
1009 EVENTS
NUMBER OF EVENTS/10°
0
20
40
60
80
100
120
160
200
0°
60°
120°
180°
240°
300°
360°
ω
1946C14

Fig. 3

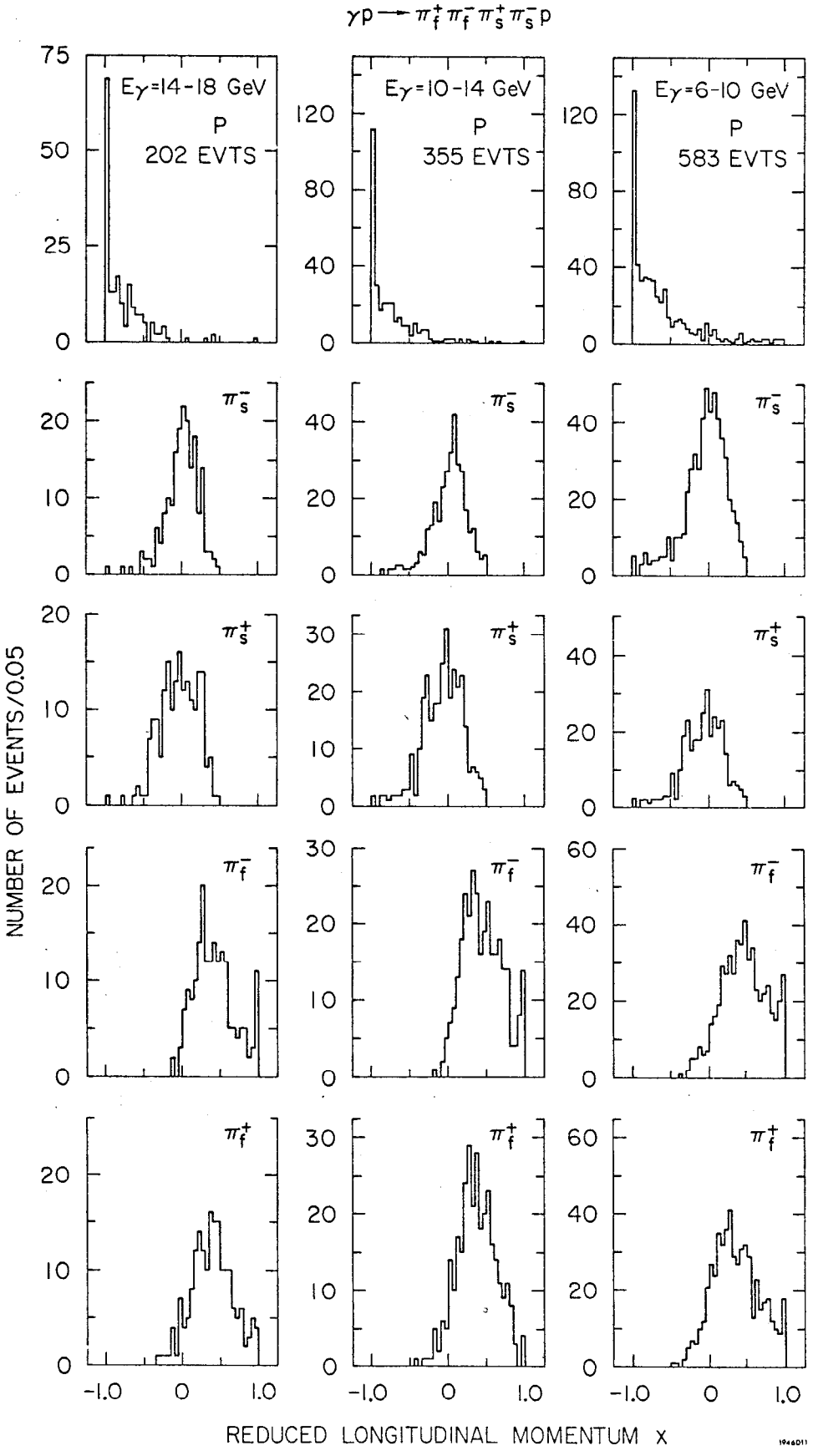
γp → π⁺f π⁻f π⁺s π⁻s p
Eγ=14-18 GeV
P
202 EVTS
Eγ=10-14 GeV
P
355 EVTS
Eγ=6-10 GeV
P
583 EVTS
π⁻s
π⁺s
π⁻f
π⁺f
NUMBER OF EVENTS/0.05
REDUCED LONGITUDINAL MOMENTUM x
-1.0
0
1.0

Fig. 4

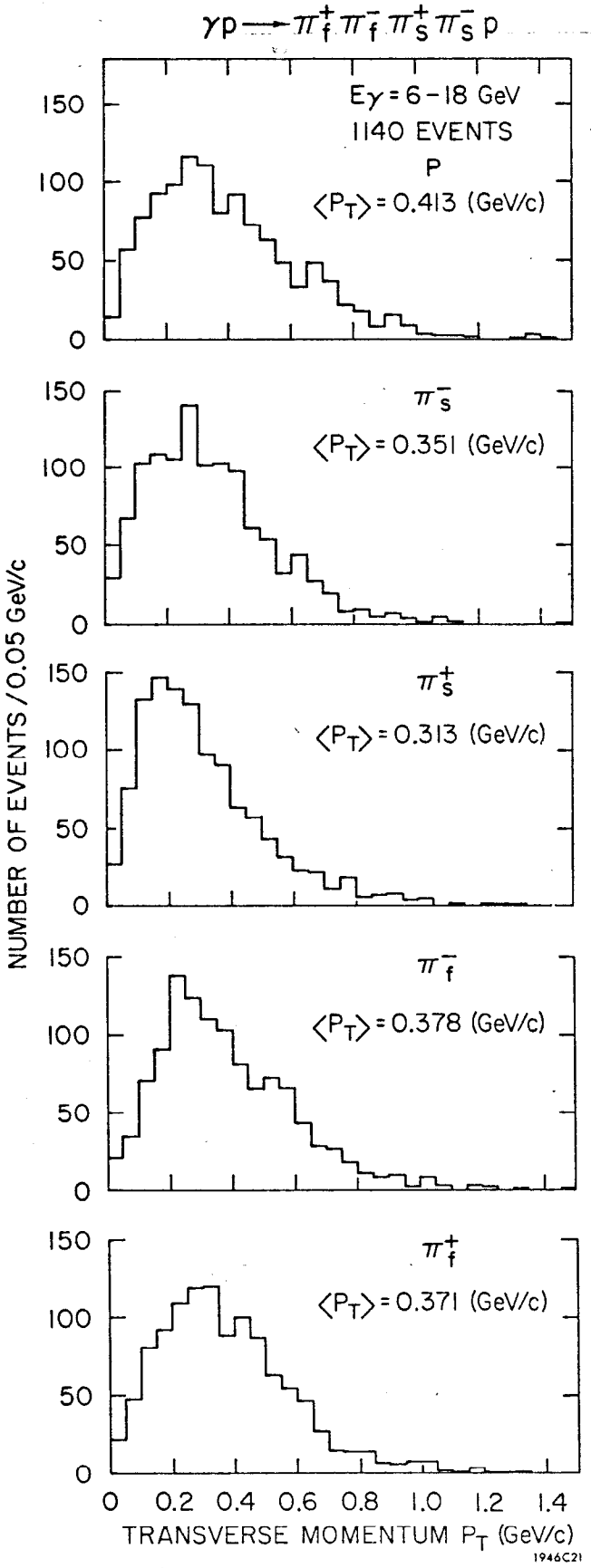
γp → π⁺f π⁻f π⁺s π⁻s p
Eγ = 6 – 18 GeV
1140 EVENTS
P
⟨PT⟩ = 0.413 (GeV/c)
π⁻s
⟨PT⟩ = 0.351 (GeV/c)
π⁺s
⟨PT⟩ = 0.313 (GeV/c)
π⁻f
⟨PT⟩ = 0.378 (GeV/c)
π⁺f
⟨PT⟩ = 0.371 (GeV/c)
NUMBER OF EVENTS / 0.05 GeV/c
150
100
50
0
0 0.2 0.4 0.6 0.8 1.0 1.2 1.4
TRANSVERSE MOMENTUM PT (GeV/c)
1946C21

Fig. 5

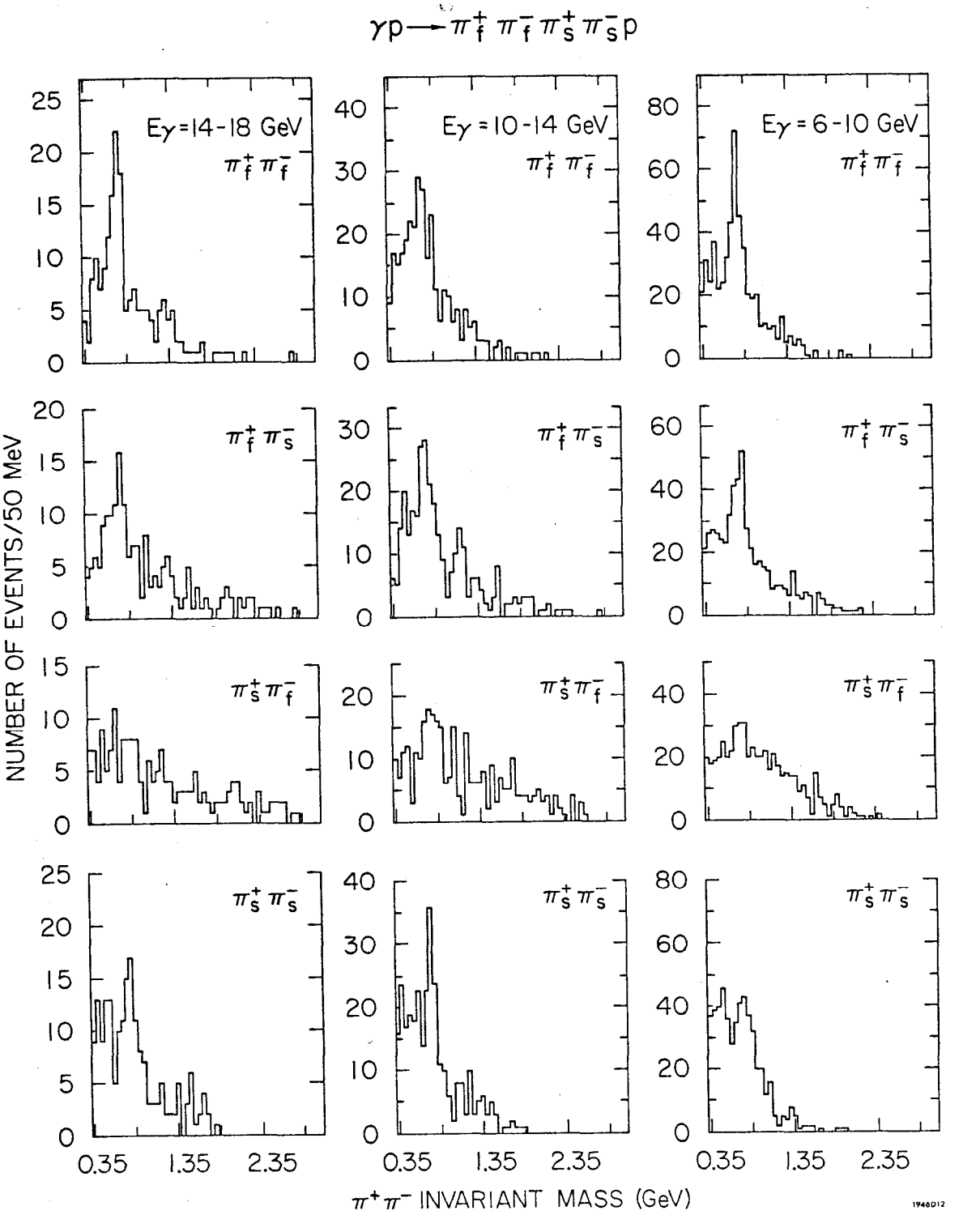
γp → π⁺f π⁻f π⁺s π⁻s p
Eγ = 14-18 GeV
Eγ = 10-14 GeV
Eγ = 6-10 GeV
π⁺f π⁻f
π⁺f π⁻s
π⁺s π⁻f
π⁺s π⁻s
NUMBER OF EVENTS/50 MeV
π⁺π⁻ INVARIANT MASS (GeV)
0.35
1.35
2.35
1946D12

Fig. 6

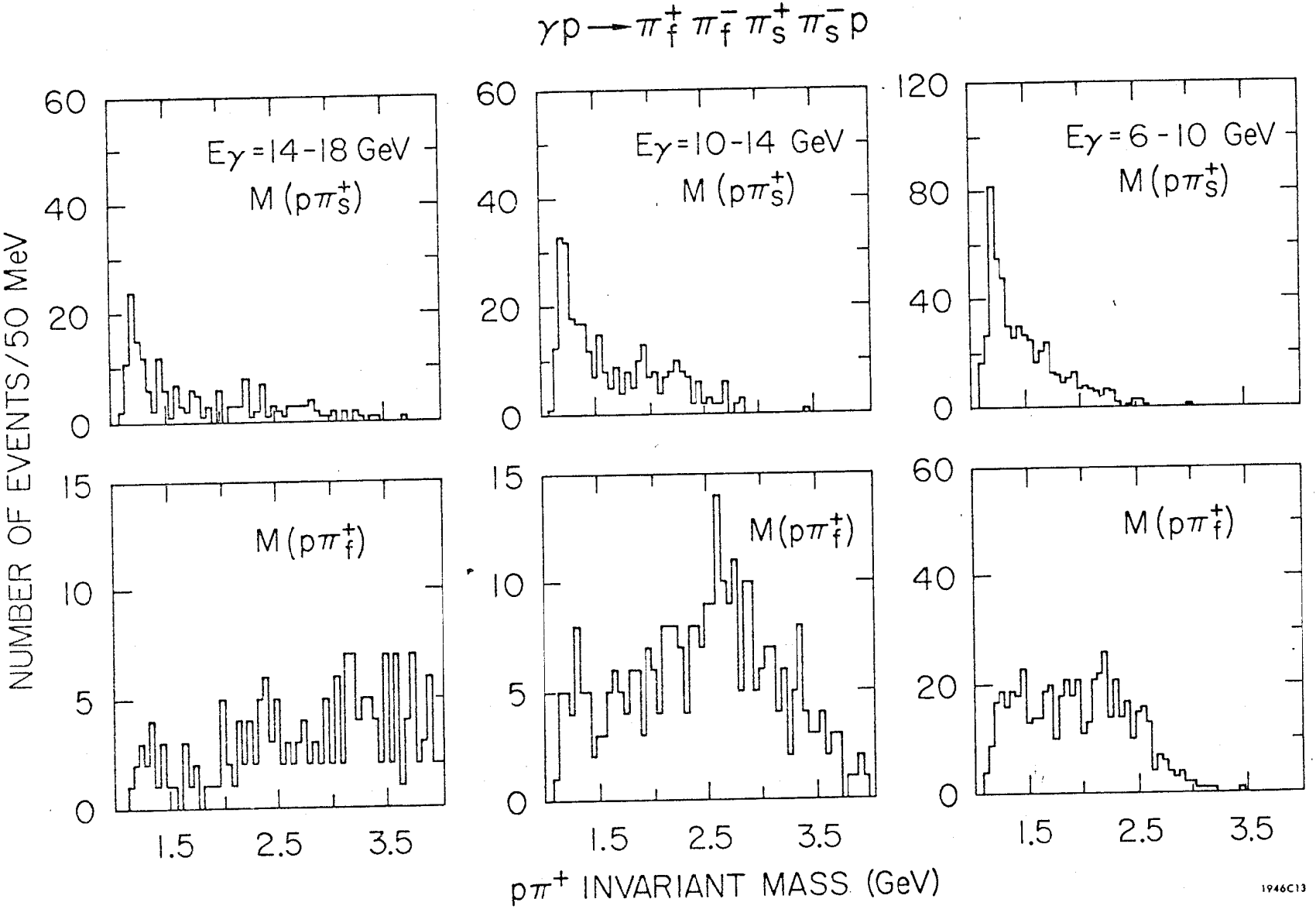
$\gamma p \rightarrow \pi_f^+ \pi_f^- \pi_s^+ \pi_s^- p$
$E\gamma = 14-18$ GeV
$M(p\pi_s^+)$
$E\gamma = 10-14$ GeV
$M(p\pi_s^+)$
$E\gamma = 6-10$ GeV
$M(p\pi_s^+)$
$M(p\pi_f^+)$
$M(p\pi_f^+)$
$M(p\pi_f^+)$
NUMBER OF EVENTS/50 MeV
$p\pi^+$ INVARIANT MASS (GeV)
1946C13

Fig. 7

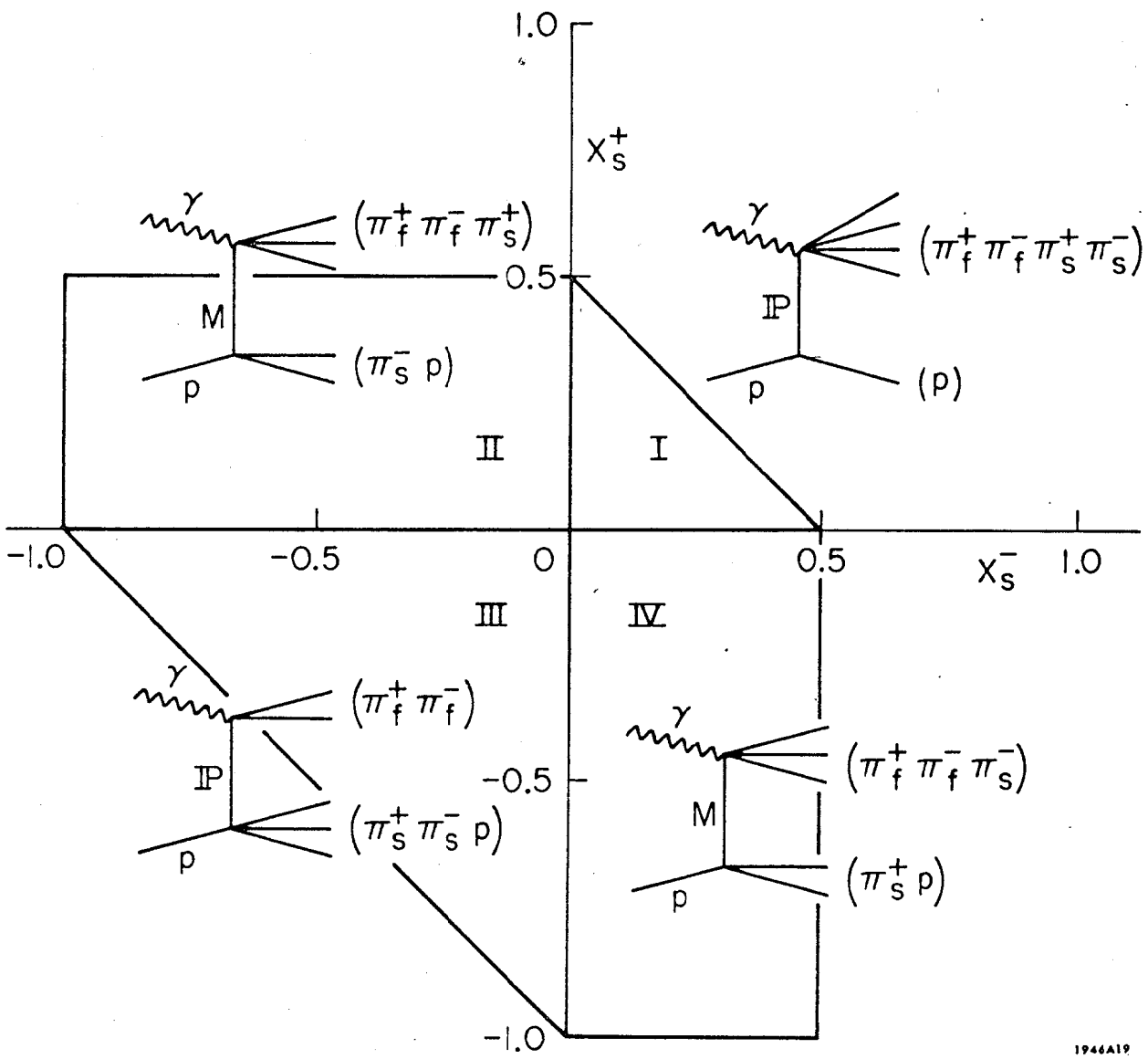
1.0
X_s^+
0.5
M
$(\pi_s^- p)$
p
$(\pi_f^+ \pi_f^- \pi_s^+)$
γ
II
I
IP
p
(p)
$(\pi_f^+ \pi_f^- \pi_s^+ \pi_s^-)$
γ
-1.0
-0.5
0
0.5
X_s^-
1.0
III
IV
γ
$(\pi_f^+ \pi_f^-)$
IP
$(\pi_s^+ \pi_s^- p)$
p
-0.5
γ
$(\pi_f^+ \pi_f^- \pi_s^-)$
M
$(\pi_s^+ p)$
p
-1.0
1946A19

Fig. 8

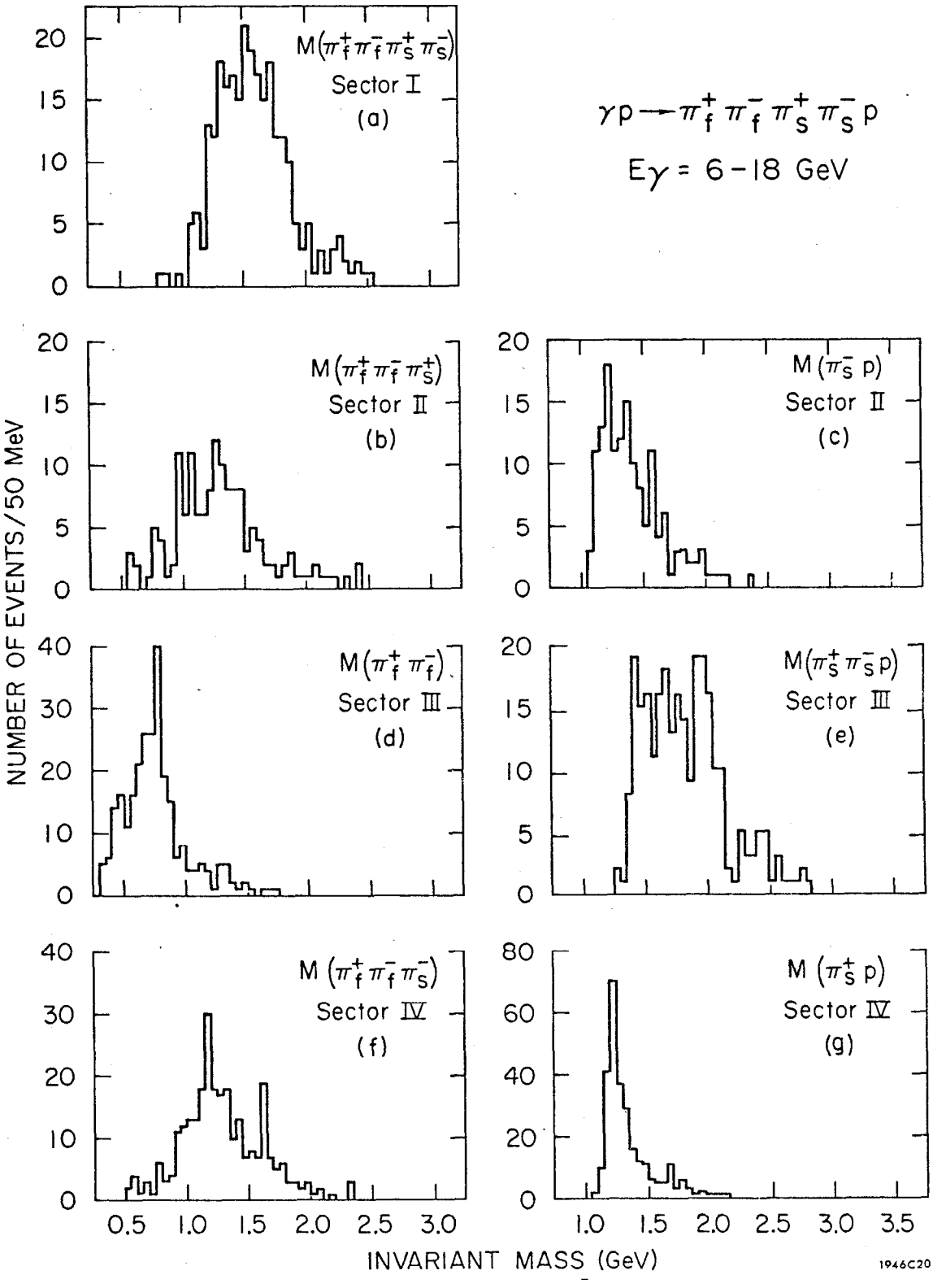
$\gamma p \rightarrow \pi_f^+ \pi_f^- \pi_s^+ \pi_s^- p$
$E\gamma = 6-18$ GeV
$M(\pi_f^+ \pi_f^- \pi_s^+ \pi_s^-)$
Sector I
(a)
$M(\pi_f^+ \pi_f^- \pi_s^+)$
Sector II
(b)
$M(\pi_s^- p)$
Sector II
(c)
$M(\pi_f^+ \pi_f^-)$
Sector III
(d)
$M(\pi_s^+ \pi_s^- p)$
Sector III
(e)
$M(\pi_f^+ \pi_f^- \pi_s^-)$
Sector IV
(f)
$M(\pi_s^+ p)$
Sector IV
(g)
NUMBER OF EVENTS/50 MeV
INVARIANT MASS (GeV)
1946C20

Fig. 9

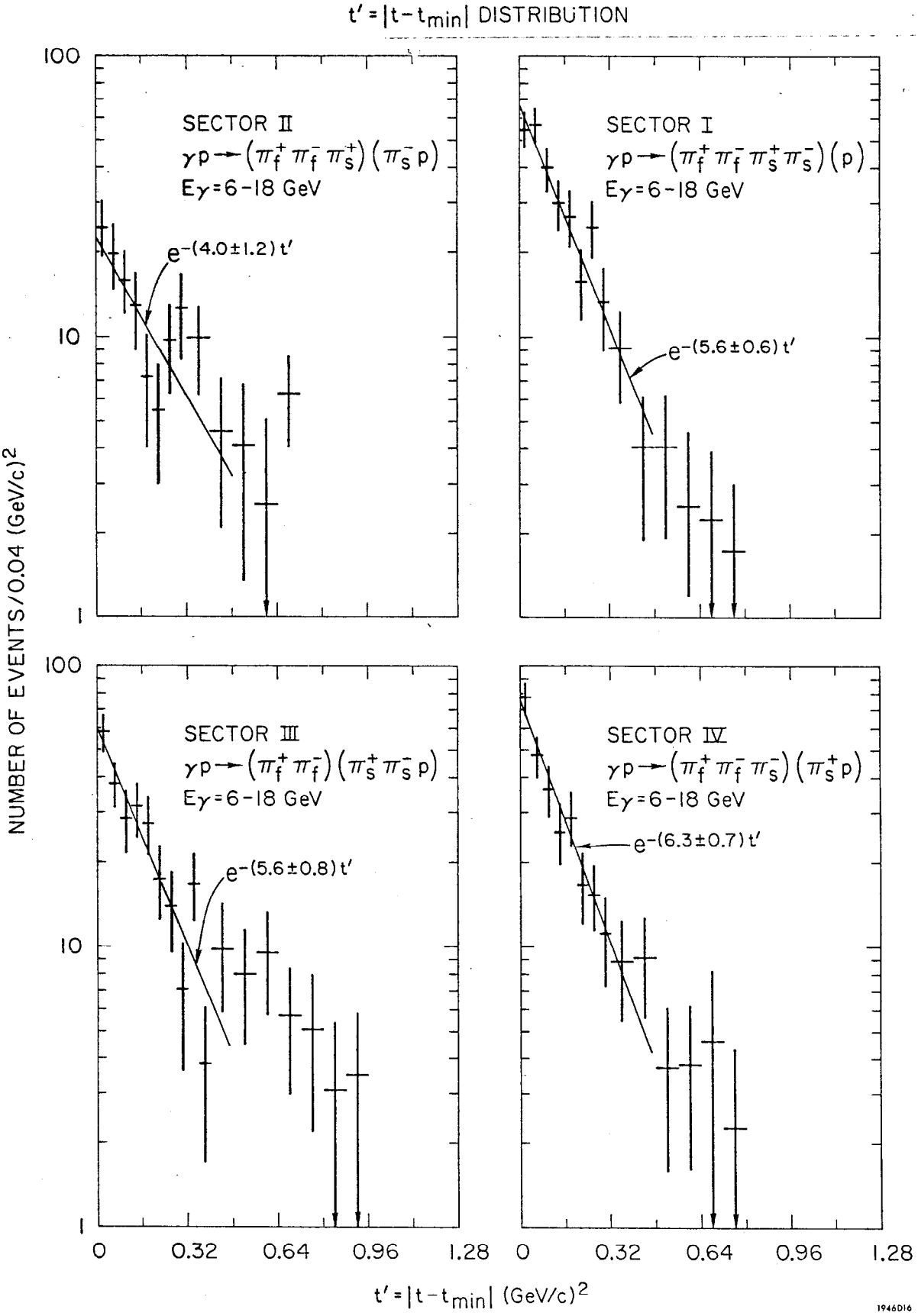
t′ = |t − t_min| DISTRIBUTION
SECTOR II
γp → (π_f^+ π_f^- π_s^+)(π_s^- p)
Eγ = 6 − 18 GeV
e^−(4.0±1.2) t′
SECTOR I
γp → (π_f^+ π_f^- π_s^+ π_s^-)(p)
Eγ = 6 − 18 GeV
e^−(5.6±0.6) t′
SECTOR III
γp → (π_f^+ π_f^-)(π_s^+ π_s^- p)
Eγ = 6 − 18 GeV
e^−(5.6±0.8) t′
SECTOR IV
γp → (π_f^+ π_f^- π_s^-)(π_s^+ p)
Eγ = 6 − 18 GeV
e^−(6.3±0.7) t′
NUMBER OF EVENTS/0.04 (GeV/c)^2
100
10
1
0
0.32
0.64
0.96
1.28
t′ = |t − t_min| (GeV/c)^2
1946D16

Fig. 10

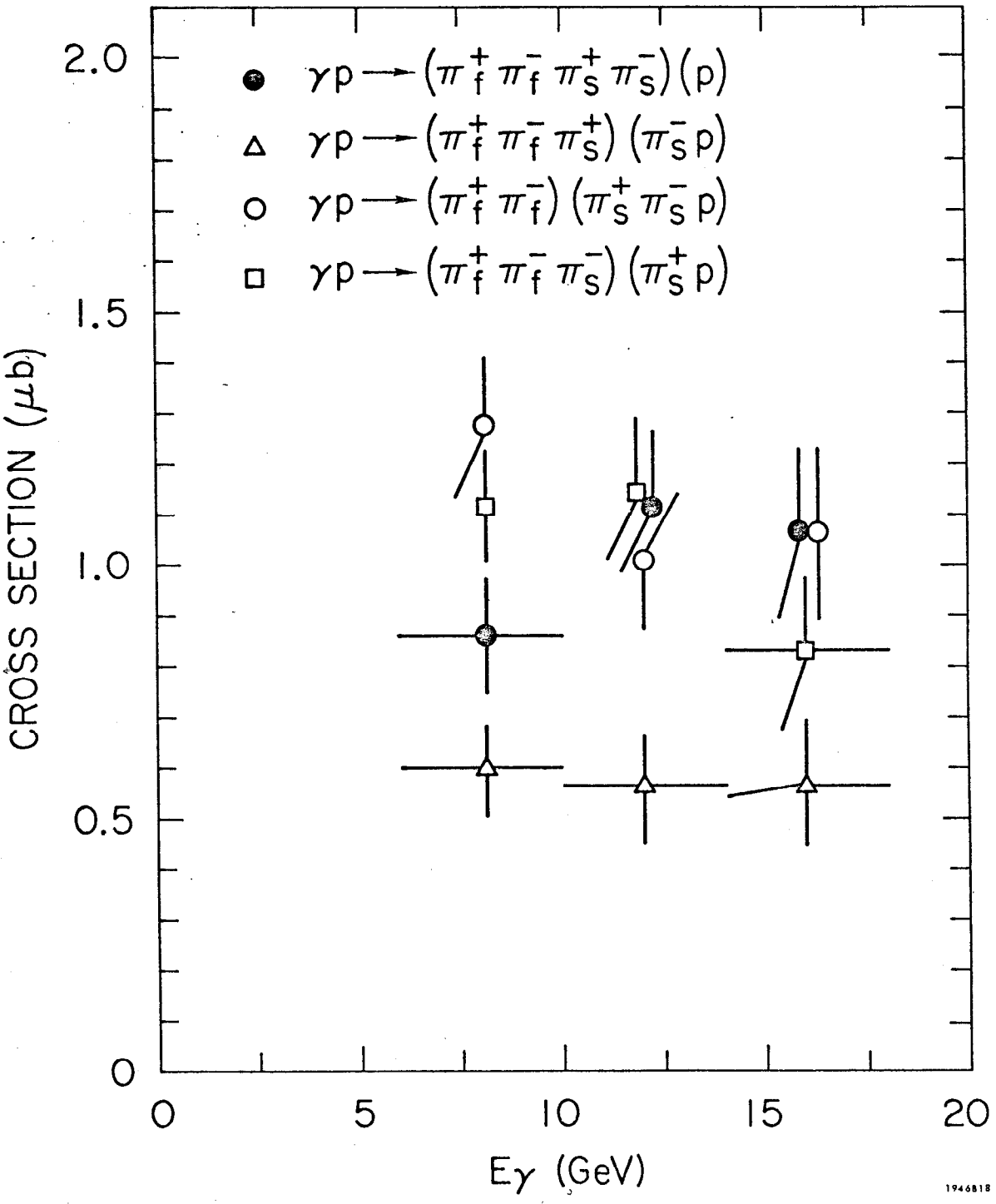
$\gamma p \rightarrow (\pi_f^+ \pi_f^- \pi_s^+ \pi_s^-)(p)$
$\gamma p \rightarrow (\pi_f^+ \pi_f^- \pi_s^+)(\pi_s^- p)$
$\gamma p \rightarrow (\pi_f^+ \pi_f^-)(\pi_s^+ \pi_s^- p)$
$\gamma p \rightarrow (\pi_f^+ \pi_f^- \pi_s^-)(\pi_s^+ p)$
CROSS SECTION (μb)
2.0
1.5
1.0
0.5
0
0
5
10
15
20
$E\gamma$ (GeV)
1946818

Fig. 11

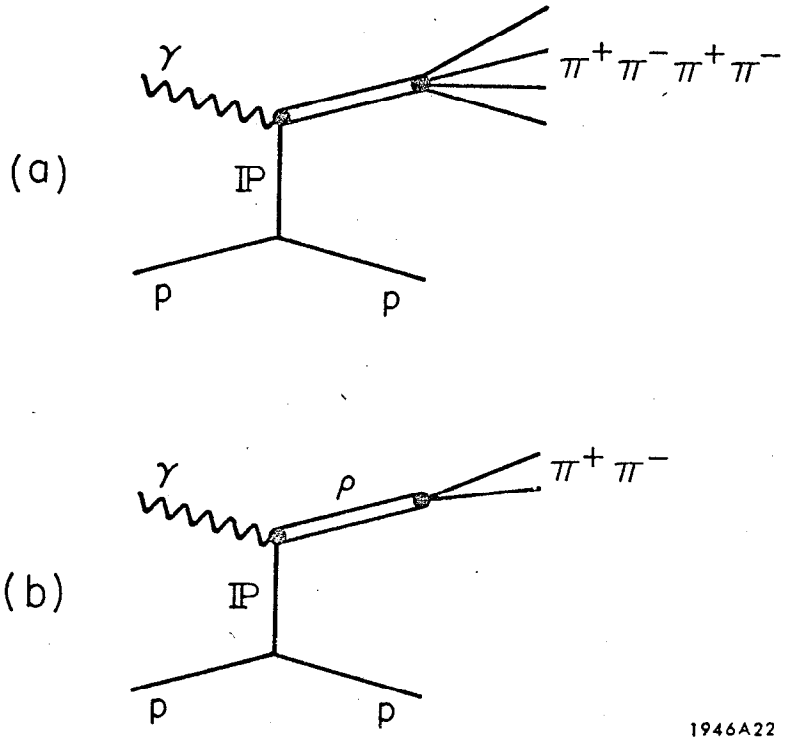

Fig. 12

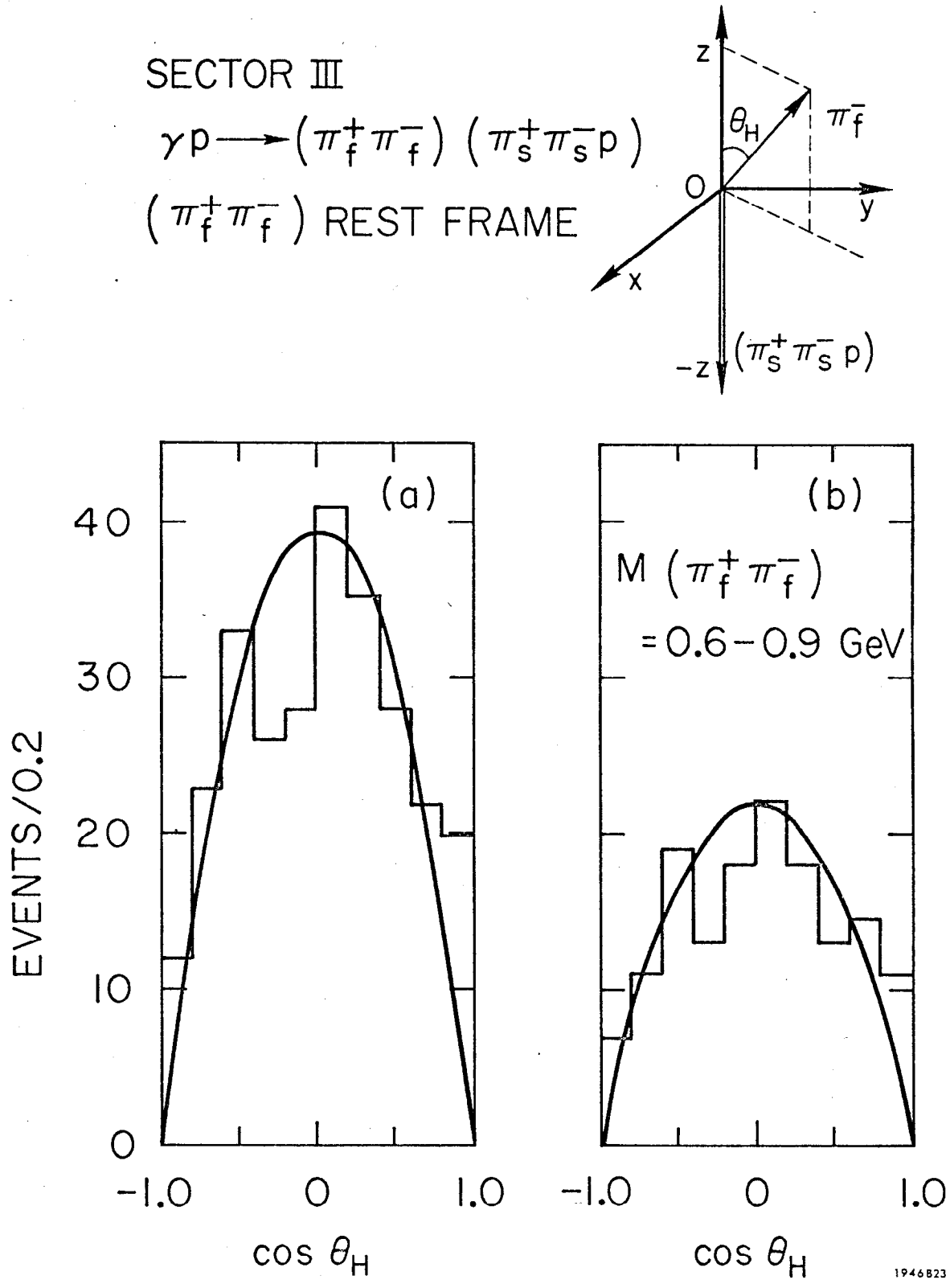
SECTOR III
$\gamma p \longrightarrow (\pi_f^+ \pi_f^-)\ (\pi_s^+ \pi_s^- p)$
$(\pi_f^+ \pi_f^-)$ REST FRAME
z
θ_H
π_f^-
O
y
x
$-z$
$(\pi_s^+ \pi_s^- p)$
(a)
(b)
$M\ (\pi_f^+ \pi_f^-)$
$= 0.6 - 0.9$ GeV
EVENTS/0.2
40
30
20
10
0
-1.0
0
1.0
$\cos \theta_H$
1946B23

Fig. 13

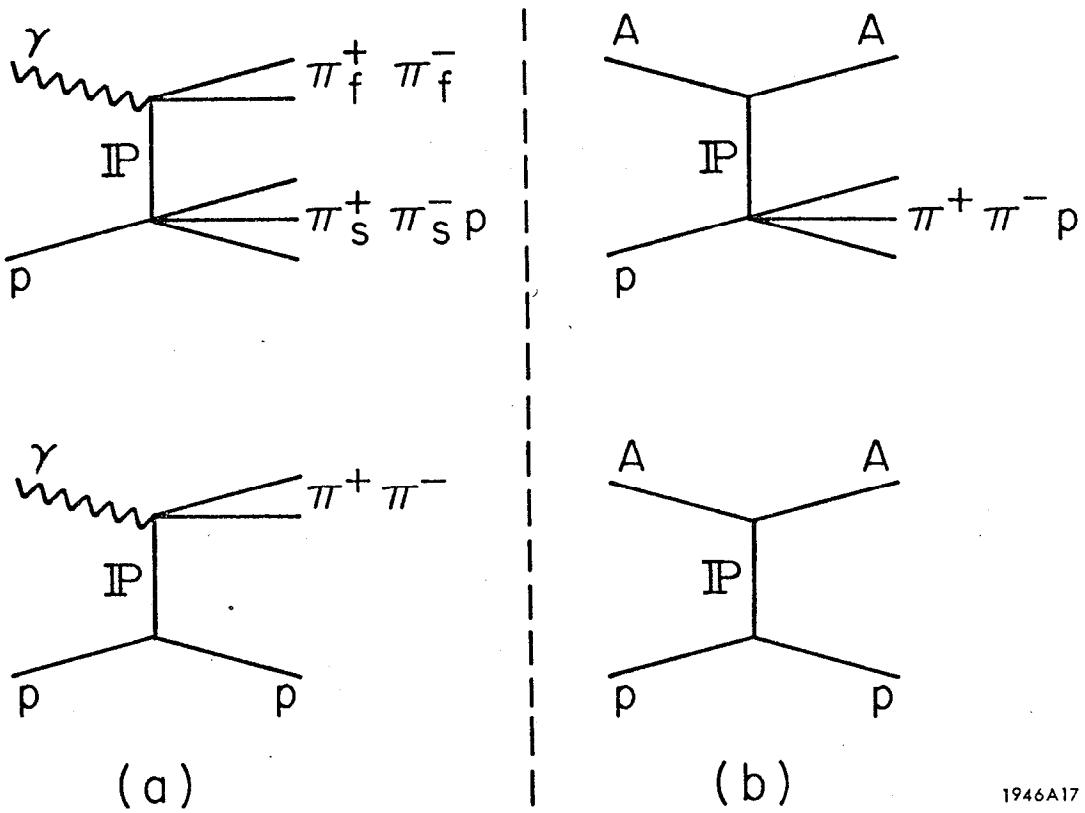
γ
π_f^+ π_f^-
IP
π_s^+ π_s^- p
p
A
A
IP
π^+ π^- p
p
γ
π^+ π^-
IP
p
p
A
A
IP
p
p
(a)
(b)
1946A17

Fig. 14